Electronic Supplementary Material (ESI) for Soft Matter.

Supporting Information for:

The role of near-wall drag effect on the dynamics of tethered DNA under shear flow

G. Nir[1,2,*], E. Chetrit[3], A. Vivante[2], Y. Garini[2] and R. Berkovich[3,4,*]

[1] Harvard Medical School, Dep. of Genetics, Boston, MA 02115, USA.

[2] Bar Ilan University, Department of Physics and Institute of Nanotechnology, Ramat Gan 52900, Israel.

[3] Ben-Gurion University of the Negev, Department of Chemical-Engineering, Beer Sheva 84105, Israel.

[4] The Ilze Katz Institute for Nanoscience and Technology, Ben-Gurion University of the Negev, Beer Sheva 84105, Israel.

Tethered Particle Motion (TPM) based microfluidic apparatus

To allow proper propagation of fully developed laminar flow, and nanometric precision detection of the end-to-end distance along the flow direction in the vicinity of a wall, we designed our fluidic system according to these two major guidelines (Figure S1A): (1) allowing continuous buffer flow in the chamber that was placed under the microscope. (2) Having a large opening to enable the ability to closely approach the flow chamber with a thick objective. This requirement evolved from the necessity to use proper dark-field illumination and a high magnification lens. The flow chamber, whose schematics and measures shown in Figure S1, was assembled by two glass coverslips, spaced with an oblong-shaped ~ 100 μm thick parafilm. The buffer was flown into the chamber through a one mm in diameter inlet hole that from which it propagated along the defined *x*- axis, and discharged through the one mm in diameter outlet located 50 mm away from the inlet.

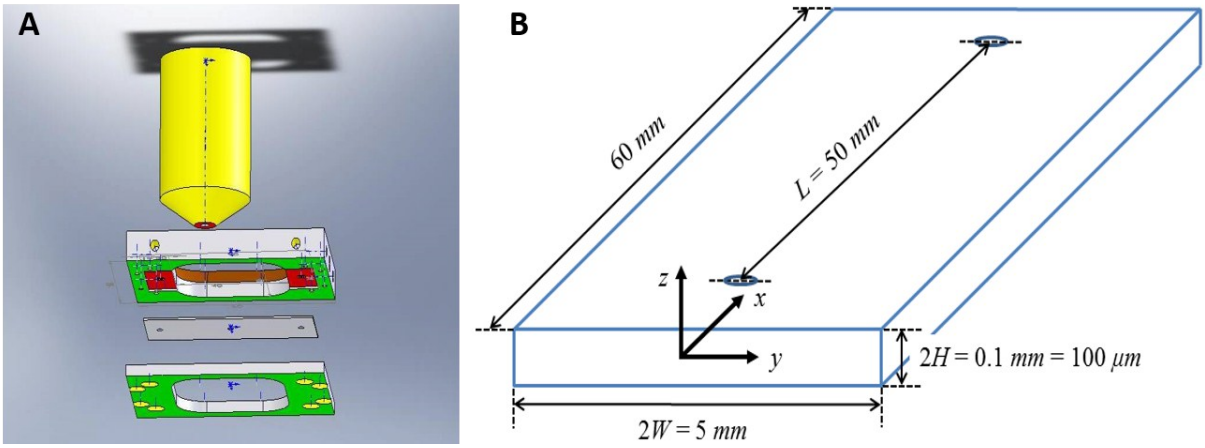

Figure S1. Fluidic chamber and holder. A. Work plans for the flow chamber and chamber holder, assuring the required space for the objective to closely approach the slides. Most of the slide surface is not covered and thus is optically open (*Shimon Filo*, Bar-Ilan University workshop). B. Geometric sketch of the microfluidic chamber, with its dimensions.

Optical principles. The two underlying principles of the TPM optical design are based on the bright illumination achieved from a gold nanoparticle due to plasmonic effects and contrast enhancement by a dark-field microscope. In TPM, the centroid position of a probe, a gold nanobead (diameter = 80 nm) in our case, is recorded over time to follow the end-to-end statistics of a polymer. To achieve higher sensitivity in detecting single gold nanobeads, we

employed dark field illumination. The guiding principle of a dark-field microscope is that only light from scattering objects (e.g. gold nanobead) penetrates into the microscope objective and creates an image, and hence the background remains dark. The light in our dark-field microscope comes from a halogen lamp (Figure 1), which travels through two parallel apertures, and reaches two tilted mirrors that direct it to hit the specimen surface at an angle. Light that impinges on a scattering object is scattered in all directions and some of it will penetrate the microscope objective and consequently imaged on an electron-multiplying (EM) charge-coupled device (CCD) camera. Another key principle in our setup is the efficient scattering of metallic nanoparticles and in particular, gold. The contribution of the imaginary part of the refractive index for such nano metallic particles can be seen in the *Rayleigh* equation for the scattered light.

Biochemical tethering of the DNA molecule and measurements. As indicated in the experimental methods section, linear dsDNAs of about 920 nm were tethered to a glass surface coated with digoxigenin (Roche), and attached to 80 nm gold nanobead at the dsDNA other edge (Figure S2A). Under the same section, we also mention imprinting gold crosses directly into the slides for accurate correction of drift, which occurs when introducing flow to the system.

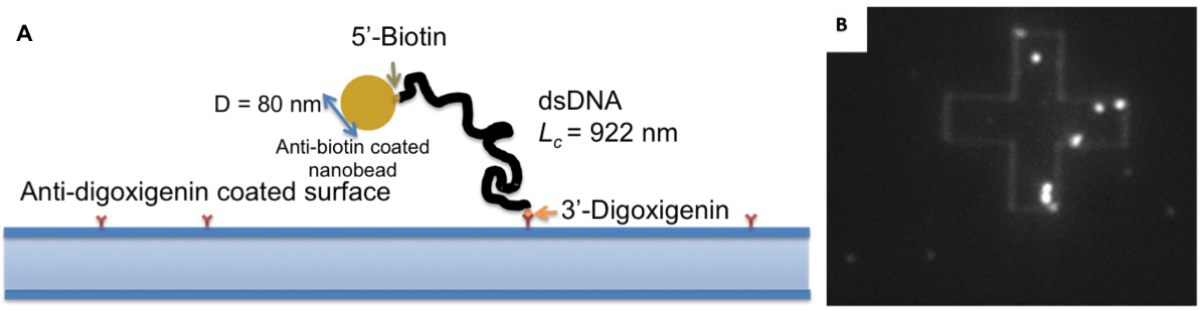

Figure S2. Tethered DNA. One edge of the dsDNA is surface tethered via dig-anti-dig specific binding whereas its other edge is bound to a gold nanobead by biotin-anti-biotin attachment. B. Gold cross imprinted on a glass slide in a typical experiment observed through a reflected dark-field microscope. The round scatters surrounding it are gold nanobeads.

The gold nanobeads centroid position (its projection in the XY plane) is recorded over time. When flow is introduced into the microfluidic environment, the cell suffers from drift that

causes the entire cell to move. To accurately correct the drift we used e-beam lithography to imprint gold crosses on the glass slide. Each cross (Figure S2B) serves as an anchoring point and represents the glass surface. A specific MATLAB (Mathworks) code was used to find the centroid position at each time-point by cross-correlating with an ideal, computer-built cross template (written by *Moshe Lindner* and *Ted Young*). To correct the drift, the change in the centroid position of the cross was reduced from the centroid position of the gold nanobead for each time point. This latter procedure enabled monitoring the bead's movement without being subjected to drift, hence achieving a detection accuracy of ±5 nanometers.

Characterization of the flow

Adequate characterization of the flow requires an exact description of the system, defining its boundaries (Figure S1B) and work assumptions, which include steady state conditions, isothermal and fully developed incompressible Newtonian flow on the direction of the x-axis. Since the measurements are recorded in the central region of the chamber, edge effects can be neglected ($H/L = 0.001 << 1$, and $H/W = 0.02 << 1$), which means that the flow profile can be estimated by a velocity profile propagating on the x-axis and varying with the z-axis, $u_x(z)$. The nature of the flow can be estimated using the *Reynolds* number (1), which is a dimensionless quantity, representing the ratio between inertial and viscous forces, and given by:

(1) $$Re = \frac{\rho D_H u}{\mu} = \frac{Q D_H}{\nu A}$$

where $D_H = 4HW/(H+W) = 1.96 \cdot 10^{-4}$ m is the hydraulic diameter of the cross-section area, $A = 4HW = 5.0 \cdot 10^{-7}$ m^2, through which the fluid flows. ν is the kinematic viscosity, given by the ratio between the viscosity, μ, and density, ρ, of the fluid. For water at room temperature, $\nu = \mu/\rho \sim 1 \cdot 10^{-6}$ m^2/s. For the flow rates that were applied in the experiments (Q = 0.1 – 15 ml/min), we calculate Re = 0.65 – 97.5. These values indicate that our system is experiencing laminar flow. This means that we can calculate the velocity profile of the flow by solving the equation of continuity (mass balance), given for incompressible fluid $\nabla \cdot u = 0$, and the equation of motion (momentum balance), also known as the *Navier-Stokes* equations, which are reduced here to $dP/dx = \mu \partial^2 u_x(z)/\partial z^2$. The volumetric flow rate, Q, induces a pressure gradient, dP/dx, along the x-coordinate. The boundary conditions that were used to solve

these equations satisfy the no-slip conditions at the interface of the fluid and the walls of the chamber, which yield a maximum at the symmetrical axis of the flow (i.e. $\partial u_x/\partial z = 0$). The final solution of the velocity profile is thus given by:

$$u = u_x = u_{max}\left[1 - \left(\frac{z}{H}\right)^2\right] \quad (2)$$

with u_{max} being the maximal velocity at the symmetry axis, $u_{max} = -H^2\Delta P/(2\mu L) = 3Q/(8HW)$. $\Delta P = P_L - P_0$, is the pressure gradient along the distance L. This solution is depicted in figure S3 with the system:

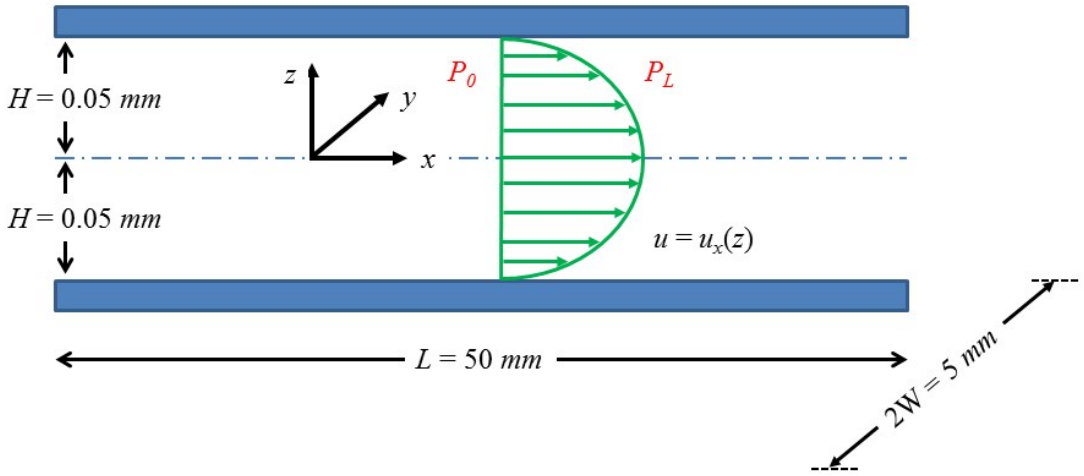

Figure S3. Illustration of the velocity profile in the experimental microfluidic setup.

Tethered polymer under shear flow near a wall

As shown in the main text, the measured dynamics of the tethered DNA-bead construct was monitored on the *x*-*y* plane (Figure S4A), recording the time dependent evolution of the molecule on these coordinates, i.e., R_x and R_y. Figure S4B shows these components.

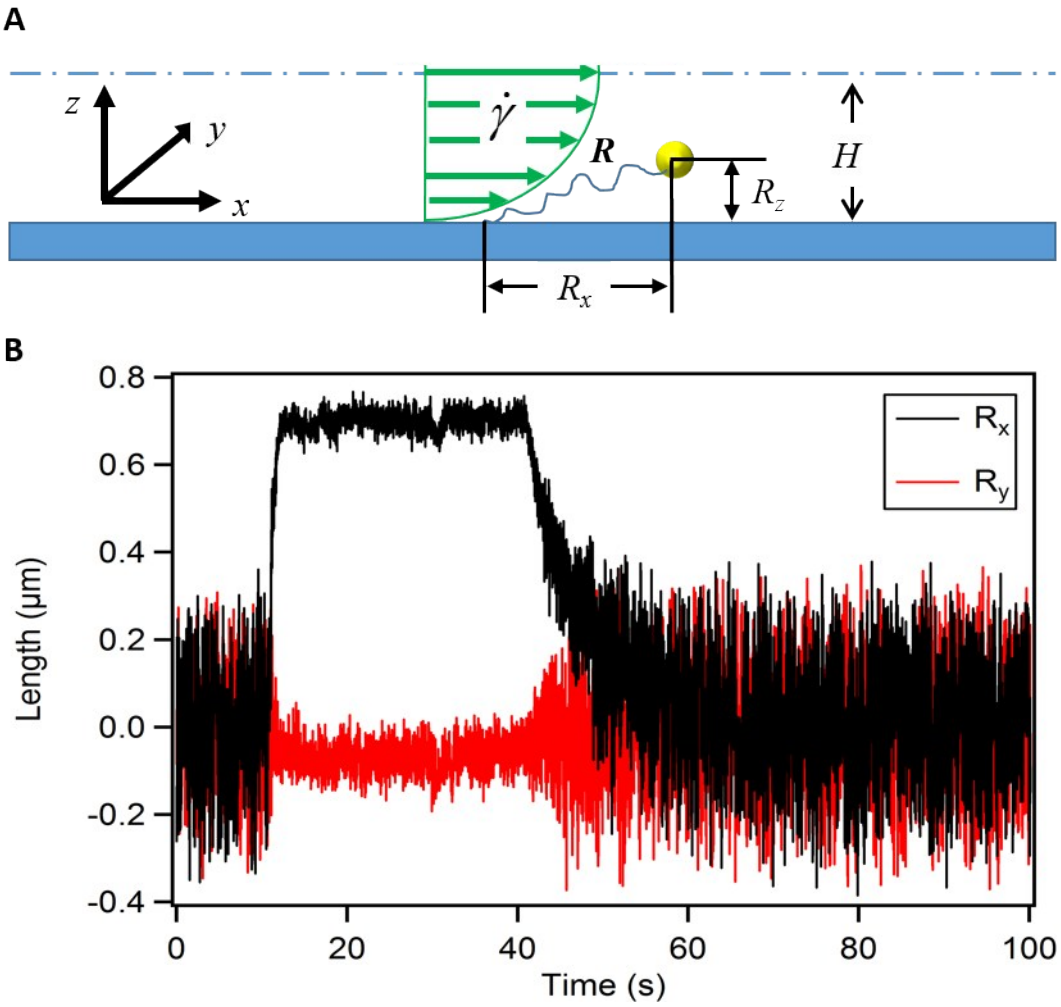

Figure S4. A. Representation of the experimental system comprised of a tethered polymer under shear force produced by the velocity profile described above. B. Time evolution of R_x (black) and R_y (red), the x and y components of the DNA-bead construct.

At the first 10 seconds, the construct fluctuates in equilibrium until 3 ml/min flow is introduced, extending the DNA chain on the *x* coordinate. This indicates that the flow is indeed laminar, and the system is stable, as no drift is observed (here as well as in the rest of the recordings). Once the chain was extended due to the flow, the fluctuations were considerably reduced on both coordinates, as can also be seen in Figure 2 in the main text. After 30 seconds under shear flow, the pump was stopped, and the chain decayed into its natural unperturbed equilibrium conformation.

Characteristic time in equilibrium

The equilibrium phase of the trajectories, where $\dot{\gamma}$ = 0, was used to determine τ. Autocorrelation function (ACF) of these regions was calculated (shown in Figure S5A), and then fitted with a single exponential according to

$$\langle R_x(t) R_x(t+\Delta t) \rangle \sim \exp(-\Delta t/\tau) \quad (3)$$

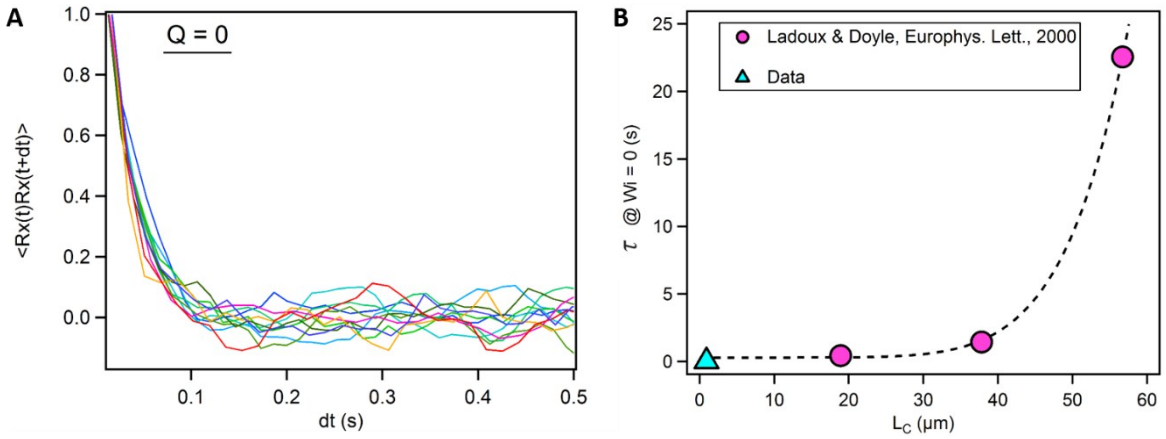

Figure S5. Estimating characteristic times in equilibrium. A. Autocorrelation functions calculated using eq. 14 from $\dot{\gamma}$ = 0 regions of the trajectories. B. Scaling of $\langle \tau_0 \rangle$ measured in this work (light blue) with L_C compared to the ones measured in ref. (2) for DNA molecules with different L_C (pink). The dashed line is plotted to guide the eye and shows a trend.

The fitted τ were then averaged over all the ACFs, returning $\langle \tau_0 \rangle$ = 0.031 ± 0.004 s. The relaxation time is known to scale with the contour length of the polymer. Comparison of our result with relaxation time of longer molecule is shown in Figure S5B. The averaged relaxation times at equilibrium for the longer DNA molecules were taken from ref. (2) and demonstrate a distinct scaling with L_C.

Perpendicular distance from the surface

The perpendicular distance from the surface, R_z, was calculated using eq. (9) from the main text, which has an implicit form. Therefore it was solved using a *Newton-Raphson* algorithm, by reorganizing the implicit expression of R_z to define the target function that satisfy $g(R_z)$ = 0:

$$g(R_z) = \left\{ L_C^2 \left(1 - \left[\frac{L_C}{4(\delta z)^{3/2}} \left\{ \frac{D_0 [f(R_z)]}{l_p \gamma \&} \right\}^{1/2} \right]^{-2/7} \right)^2 - \langle R_x \rangle^2 \right\}^{1/2} - R_z^2 \quad (4)$$

Defining,

$$W_i^* = \frac{L_C}{4(\delta z)^{3/2}} \left(\frac{D_0}{l_p \gamma \&} \right)^{1/2}, \quad (5)$$

eq. (4) can be written more conveniently as:

$$g(R_z) = \left(L_C^2 \left[1 - \left\{ W_i^* [f(R_z)]^{1/2} \right\}^{2/7} \right]^2 - \langle R_x \rangle^2 \right)^{1/2} - R_z^2 \quad (6)$$

This technique is a gradient based, and therefore requires taking the derivative of eq. (6) to write the iterative formulation of the *Newton-Raphson* method:

$$R_z(j+1) = R_z(j) - \frac{g[R_z(j)]}{g'[R_z(j)]}. \quad (7)$$

Eq. (7) was solved numerically for an array of initial guesses ranging from R_z = 0.04 μm to 1.00 μm iteratively, until converging under a predefined tolerance of ε = 0.001. From the converged solutions, the one with the minimal error, dR_z, was chosen:

$$dR_z = \sqrt{\left(\frac{\partial R_z}{\partial D_0} dD_0 \right)^2 + \left(\frac{\partial R_z}{\partial f} df \right)^2 + \left(\frac{\partial R_z}{\partial \langle R_x \rangle} \delta z \right)^2} \quad (8)$$

$$dR_z = \left\{ [X f(R_z) dD_0]^2 + (X D_0 df)^2 + \left(-\frac{\langle R_x \rangle}{R_z} \delta z \right)^2 \right\}^{-1/2} \quad (9)$$

where

$$X = \left\{ \frac{L_C^2 W_i^*}{7 R_z l_p \gamma \& [f(R_z)]^{1/2}} \right\} \left(1 - \left\{ W_i^* [f(R_z)]^{1/2} \right\}^{2/7} \right) \left\{ W_i^* [f(R_z)]^{1/2} \right\}^{9/7} \quad (10)$$

The *Faxén* correction factors calculated at the estimated R_z are shown in Figure S6, showing their asymptotic increase to unity as R_z grows. This indicates the effect of the wall proximity dramatically decrease with the extension of the DNA-bead complex via the increasing flow rates, however, it does not vanish.

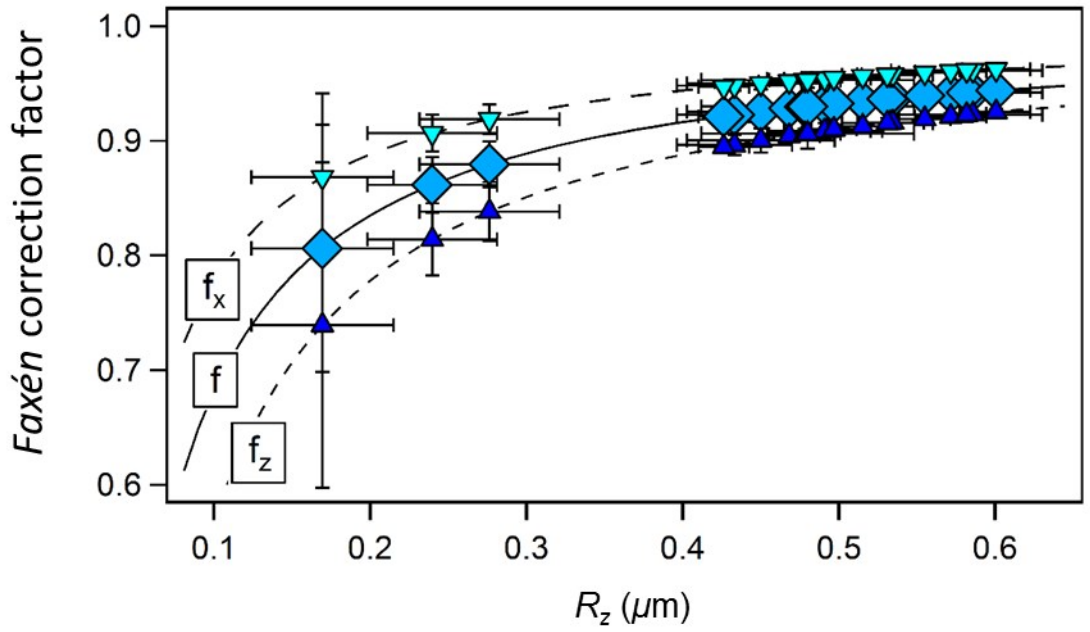

Figure S6. *Faxén* correction factors as a function of the R_z, the perpendicular distance from the surface.

References

1. Reynolds, O. 1883. An experimental investigation of the circumstances which determine whether the motion of water shall be direct or sinuous, and of the law of resistance in parallel channels. Philosophical Transactions of the Royal Society 174:935-982.
2. Ladoux, B., and P. Doyle. 2000. Stretching tethered DNA chains in shear flow. EPL 52:511.
3. Khatri, B. S., K. Byrne, M. Kawakami, D. J. Brockwell, D. A. Smith, S. E. Radford, and T. C. B. McLeish. 2008. Internal friction of single polypeptide chains at high stretch. Farad. Discuss. 139:35-51.
4. Marko, J. F., and E. D. Siggia. 1995. Stretching dna. Macromolecules 28:8759-8770.
5. Bustamante, C., J. Marko, E. Siggia, and S. Smith. 1991. Entropic Elasticity of lambda-Phage DNA. Proc. Nati. Acad. Sci USA 88:10009.
6. Happel, J., and H. Brenner. 1983. Low Reynolds number hydrodynamics: with special applications to particulate media. Springer Science & Business Media.
7. Smith, D. E., H. P. Babcock, and S. Chu. 1999. Single-Polymer Dynamics in Steady Shear Flow. Science 283:1724-1727.
8. Doyle, P. S., B. Ladoux, and J.-L. Viovy. 2000. Dynamics of a tethered polymer in shear flow. Phys. Rev. Lett. 84:4769.